Chapter 80
Triply Periodic Minimal Surface-Based Porous Scaffold Design and Analysis Subjected to Hard Tissue Reconstruction

Verma Rati, Nishant Singh, Sanjay Rai and Shekhar Kumta

Abstract Porous structures based on triply periodic minimal surfaces (TPMS) have occurred as appropriate candidates for scaffold design with high level of porosity and promising strength for bone replacement. This work describes a suitable procedure for design and modeling of 3D architecture of TPMS-based gyroid and primitive structures and identifying the optimal architecture for scaffold designing. Different models with varying porosity were reconstructed and analyzed to access the effective elastic moduli and compressive strength of each model. An optimal model that can be utilized in bone tissue replacement is identified eventually. Ti6Al4V which is considered as the best material for producing implants in conjunction with biocompatibility and strength is used in the study. The compression test performed by FEM revealed that the scaffold models with porosity level of 65 and 60% are best suited for cortical bone replacement and the model with 90% porosity can be used on the anatomical location, which are more inclined to cancellous bones.

Keywords Tissue engineering · Porous scaffolds · TPMS · Gyroid · Primitive · Finite element analysis

V. Rati · S. Rai (✉)
School of Biomedical Engineering, IIT BHU, Varanasi, India
e-mail: skrai.bme@iitbhu.ac.in

V. Rati
e-mail: rati.verma14@gmail.com

N. Singh
Department of Biomedical Engineering, NIT Raipur, Raipur, Chhattisgarh, India
e-mail: nksingh.bme@gmail.com

S. Kumta
Department of Orthopaedics and Traumatology, Prince of Wales Hospital,
the Chinese University of Hong Kong, Shatin, New Territories, Hong Kong
e-mail: shekharkumta@gmail.com

80.1 Introduction

The field of tissue engineering aims to develop an efficient biological substitute in order to preserve, maintain, or enhance the function of tissue. Scaffolds play a significant part in deciding mechanical characteristics of desired tissue formed in it at a macroscopic or microscopic scale and also provides the vascularization needed by the newly forming tissues [1]. Scaffold must be biocompatible, bio-inert, bioactive, bioresorbable, and biodegradable so as to work efficiently to possess long term results [2]. Porous scaffold, therefore, provides necessary temporary atmosphere for adhesion, propagation, and differentiation of cell [3], together with the transport phenomena and degradation behavior [4]. Other advantages of these porous scaffolds include its flexibility in terms of mechanical properties, a large surface area that enables bio-functionalization and infection prevention and accelerates bone ingrowth as well as facilitates drug delivery in implants [5]. To establish a balance between the mechanical properties of scaffold and porosity is a challenge [1, 6]. Tissue regeneration efficiency is greatly affected by scaffold pore size [3].

Triply periodic minimal surface (TPMS) is an emerging area of interest for designing the scaffolds because of its unique properties like the ability to mimic the organic system and to build self-supportive structures for additive manufacturing [7, 8]. Another reason for TPMS-based scaffolds to draw the attention toward it is because of its capability to provide site-specific biological performance [9]. TPMS is defined in mathematical terms as surface curvatures which are infinite and periodic in 3D Euclidian space that owes to a surface capable of generating highly controllable and homogeneous scaffold design [10]. TPMS have implicit periodic surfaces in three independent Cartesian directions with mean curvature equal to zero [11]. These minimal surfaces play a very essential role in guiding chemical, cellular, and biochemical processes [10]. The TPMS-based porous structures have the potential to attain the lightweight bone models and medical requirements of bone tissue, thus providing a solution for the production of biomimetic bone in biomaterials and tissue engineering [12].

Observing the TPMS topology for Schoen's gyroid that perfectly suits the porous-solid structural configuration ideal for tissue engineering scaffolds [4, 13–16], this paper emphasizes on TPMS surface geometry and gyroid surface, particularly.

The present study aims to develop a porous scaffold based on TPMS geometry that possesses the mechanical properties (elastic modulus and compressive strength) proximate to bone. The study utilizes Schwarz's primitive (P) and Schoen's gyroid surface (G) structures to design bone scaffolds as their macroscopic structure is analogous to bone. Ti6Al4V (Grade 5) regarded as a biocompatible material is employed with its mechanical properties with scaffold porosities within the range of 60–90%. Unit cell length and pore size are varied with wall thickness kept constant at 102 μm for G and 133 μm for P, respectively, to achieve porosities within the desired range for both the structures (P and G). Finite element analysis was performed in ANSYS® software with static loading and boundary conditions for the

determination of compressive strength based on von-Mises criteria to study the deformation behavior and to estimate the effective elastic moduli and compressive yield strength.

80.2 Materials and Method

80.2.1 TPMS-Based Porous Scaffold-Primitive (P) and Gyroid (G) Surface Modeling

Both the primitive (P) as well as gyroid surface are designed from the basic parametric equations with implicit functions described in Eqs. (80.1) and (80.2).

$$\text{Primitive } (P): \cos{(x)} + \cos{(y)} + \cos{(z)} = 0 \tag{80.1}$$

$$\text{Gyroid: } \sin{(x)} * \cos{(y)} + \sin{(y)} * \cos{(z)} + \sin{(z)} * \cos{(x)} = 0 \tag{80.2}$$

The unit cell of TPMS is designed with a MATLAB code, executed in the MATLAB$^{\circledR}$ (v. R2016a) software. "MESHGRID" command along with "ISOSURFACE" command was used to extract the isosurface 3D data from the volume 3D data generated by "MESHGRID" command.

The unit cell was extended periodically in x, y, and z directions by modulating the Eqs. (80.1) and (80.2) as described in Eqs. (80.3) and (80.4) [17].

$$\text{Primitive } (P): F_P = \left[\cos{\left(\frac{2\pi Nx}{L} \right)} + \cos{\left(\frac{2\pi Ny}{L} \right)} + \cos{\left(\frac{2\pi Nz}{L} \right)} \right] - P \tag{80.3}$$

$$\text{Gyroid: } F_G(x, y, z) = \left[\sin{\left(\frac{2\pi Nx}{L} \right)} * \cos{\left(\frac{2\pi Ny}{L} \right)} + \sin{\left(\frac{2\pi Ny}{L} \right)} * \cos{\left(\frac{2\pi Nz}{L} \right)} \right.$$
$$\left. + \sin{\left(\frac{2\pi Nz}{L} \right)} * \cos{\left(\frac{2\pi Nx}{L} \right)} \right] - P$$
$$\tag{80.4}$$

where N defines the number of unit cells, L is length of the unit cell, and P is the strut thickness parameter that controls the volume fraction in a unit cell. For a scaffold with 3 × 3 × 3 unit cells (Fig. 80.1), value of N was fixed at $N = 3$, unit cell length L was varied due to which the pore diameter and total scaffold length were altered accordingly as listed in Table 80.1. Seven models for each surface (primitive: P_1–P_7 and gyroid: G_1–G_7) type were designed. As a result, a total of fourteen models were designed. P is kept constant at $P = 0$ to fix the volume fraction at 50%. "STLWRITE" command was added to the MATLAB code to export the geometry as stl file which can be imported to other software for finite element analysis (FEA).
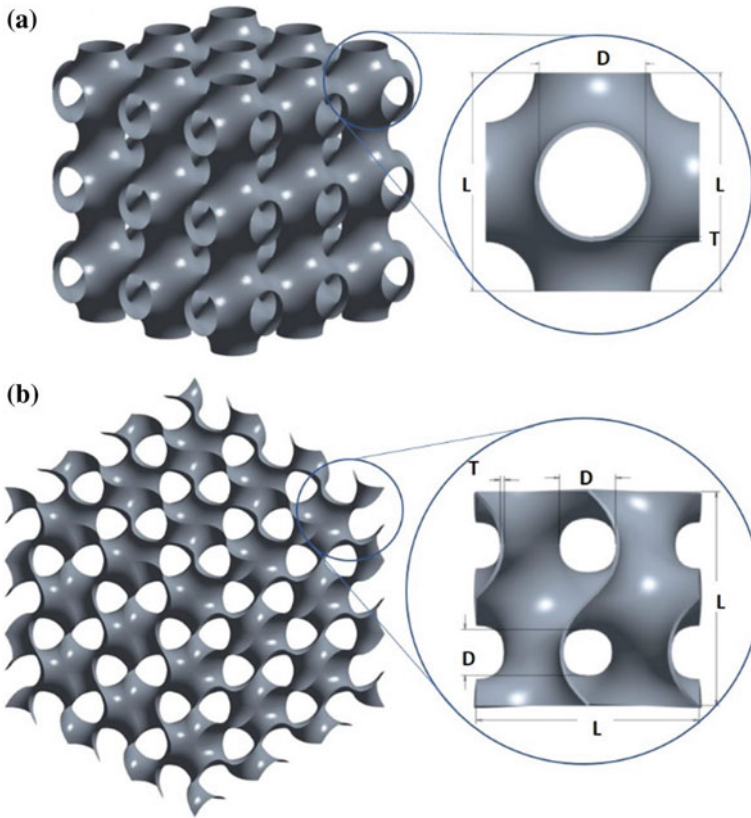
Fig. 80.1 Designed TPMS-based porous surface models. Isometric view with $3 \times 3 \times 3$ unit cells for **a** primitive surface, **b** gyroid surface (Zoom in view inside the circle presents the unit cell length (L), pore diameter (D) and wall thickness (T) of each model)

Table 80.1 Parametric values of TPMS-based primitive (P_1–P_7) and gyroid (G_1–G_7) structures

	P_1, G_1	P_2, G_2	P_3, G_3	P_4, G_4	P_5, G_5	P_6, G_6	P_7, G_7
Porosity (%)	90	85	80	75	70	65	60
Unit cell length (L) (μm)	3141	2104	1570	1256	1055	911	791
Pore size (D) (μm)	1654	1074	776	600	488	407	340

80.2.2 Design and Formulation of Finite Element Model for FEA

The surface models of P surface and gyroid were imported in 3-matic software as stl files and fixed for any errors in the surface. Wall thickness was developed and the model was exported to ANSYS software for FEA after performing surface and volume meshing. The complete procedure is explained in the following subsections.

Developing wall thickness and preparing Finite Element Models

Stl files generated through MATLAB software were imported in 3-matic software for assigning wall thickness to the surface and carrying out surface and volume meshing. The surface of the models of gyroid and P were thickened with a uniform offset of 102 µm and 133 µm, respectively (Fig. 80.1). Since, offsetting the surface disturbed the surface geometry (mesh) of gyroid structures, surface meshing was performed with specific 3-matic tools to improve the quality of surface mesh. Additionally, to reduce the density of the triangles and improve the quality of mesh, quality preserving reduce triangles tool followed with uniform meshing with a target triangle edge length of 0.2 was performed in a manner that element quality is preserved. The shape-quality threshold and maximum geometrical error values were fixed to 0.5 and 0.05, respectively [7].

The generated models were checked for errors and fixed accordingly. Consequently, the number of inverted normal, noise shells, bad contours, planar holes, overlapping triangles, and intersecting triangles present in each model were fixed manually to obtain a single shell with no errors. Volume meshing was done to solidify the surface models with voxel size of Tet4 elements. The volumetric models of all scaffolds generated in 3-matic software were imported to Ansys software as stl files.

Assigning Material properties, Boundary conditions, and Load parameters

Ti6Al4V (Grade 5) material considered suitable in terms of a compatible biomaterial for implants is used for FEA [18]. The elastic isotropic material properties of Ti6Al4V adopted in the study include Young's modulus of 114 GPa, Poisson's ratio of 0.33, density of 4.43 g/cc, and compressive yield strength of 1070 MPa [19].

Remeshing with 4-node SHELL181 hexahedral element was performed for each model (Fig. 80.2). Two rigid plates are fixed at the top and bottom of each scaffold to assign the boundary conditions and loading. The bottom plate is constrained in all directions while a static compressive load of 75 N is applied in negative Y direction at the top plate (Fig. 80.3).
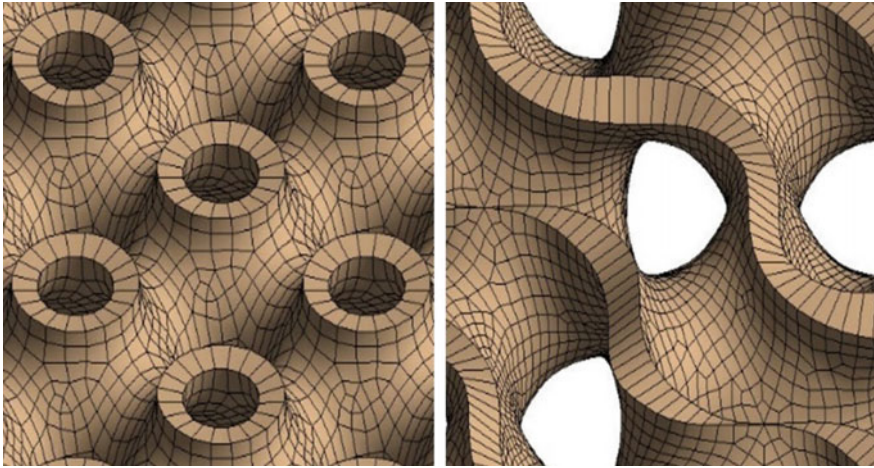
Fig. 80.2 Remeshed models with four-node hexahedral elements for primitive (left) and gyroid (right) surfaces
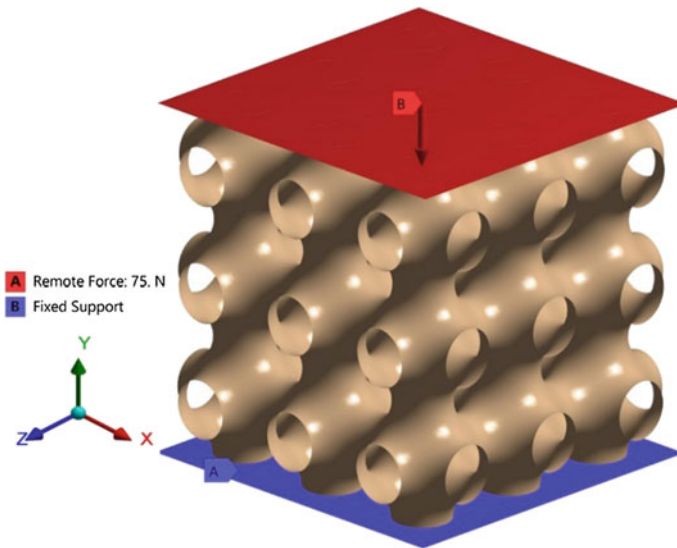

Fig. 80.3 Application of boundary conditions and load parameters. Two rigid plates, red and blue are fixed at top and bottom of designed scaffold structure and compressive load of 75 N is applied in negative Y direction

Table 80.2 Porous volume (V_P) and solid volume (V_S) of primitive (P_1–P_7) and gyroid (G_1–G_7) models

	P_1	P_2	P_3	P_4	P_5	P_6	P_7
(V_P) (μm^3)	2897.9	1287.9	763.62	495.08	348.26	260.81	195.89
(V_S) (μm^3)	28333.5	8395.1	3832.3	2000.8	1180.2	764.9	497.9

	G_1	G_2	G_3	G_4	G_5	G_6	G_7
(V_P) (μm^3)	3123.7	1402.2	780.92	499.79	352.65	262.7	198.37
(V_S) (μm^3)	31006490	9325.9	3875.8	1984.2	1176.2	756.207	496.191

80.3   Porosity

Porosity was calculated from the relation expressed in Eq. (80.3) [20].

$$N = 1 - \left(\frac{V_P}{V_S} \right) \qquad (3)$$

where V_S is the solid volume and V_P is the volume of porous construct. The solid volume constitutes the total volume of cubic construct. Solid volume (V_S) and porous volume (V_P) were calculated all primitive (P_1–P_7) and gyroid surface (G_1–G_7) models with different porosity levels (60–90%) as listed in Table 80.2.

80.4   Results

The effective elastic modulus as well as compressive strength was calculated for each model. Effective elastic moduli were determined from Hooke's law ($\sigma = \varepsilon E$) and compressive strength was obtained from von-Mises criteria. The performance characteristics of scaffold structure with $3 \times 3 \times 3$ unit cells were observed under static compressive load of 75 N. Total von-Mises stress distribution and maximum deformation were measured for scaffolds with varying length and porosity (Fig. 80.4). Compressive strength for each model was determined by the load of 75 N that caused the maximum stress of 909.24 and 1102.5 MPa in P surface model and gyroid surface model, respectively, with 70% porosity (Fig. 80.4a, b). Maximum deformation of 28.542 and 22.875 µm was obtained for P surface model and gyroid surface model, respectively, with 70% porosity (Fig. 80.4c, d). Variation in elastic modulus and compressive strength with respect to porosity has been plotted (Fig. 80.5).
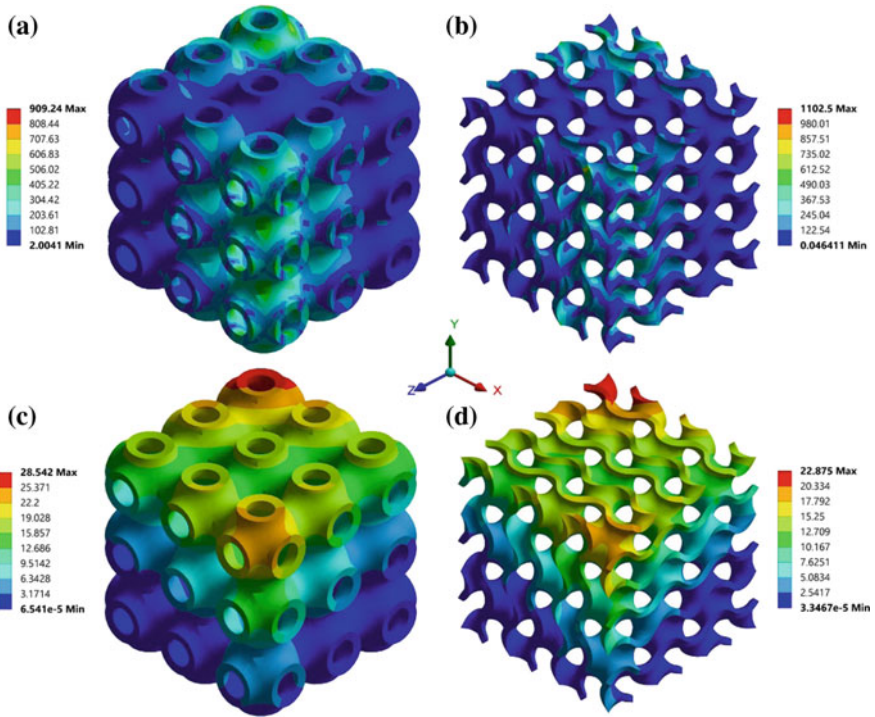
Fig. 80.4 Mechanical properties of scaffolds with 70% porosity obtained from FEA simulation. Von-Mises stress distribution (MPa) for **a** primitive structure: P_5, **b** gyroid structure: G_5 and total deformation (μm) for **c** primitive structure: P_5, **d** gyroid structure: G_5
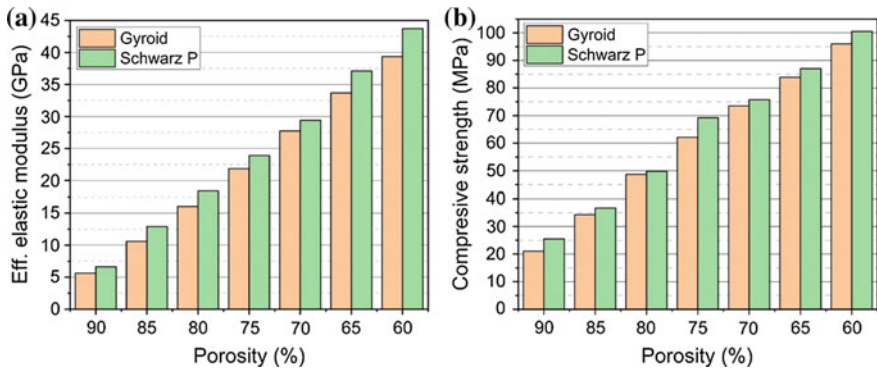

Fig. 80.5 Graphical representation of mechanical properties plotted against porosity. Plot of **a** effective elastic moduli and **b** compressive strength with respect to porosity for Schwarz P surface and gyroid surface

80.5 Discussion

Numerous studies have been carried out the design and manufacturing of TPMS-based porous scaffold materials because of the challenges imposed in this field [9, 20–22]. In order to obtain a scaffold that perfectly mimics mechanical properties similar to bone, the effective elastic moduli in addition to compressive strength of the scaffolds are obtained proximate to the bone [23, 24]. Elastic modulus for cortical bone has been noted in the range of 3–30 GPa, whereas for cancellous bone, it is in the range of 0.02–0.2 GPa. Also, the compressive strength for cortical and cancellous bone is reported as 100–230 MPa and 2–12 MPa, respectively [25]. Although, the mechanical characteristics of bone with compressive load show a discrepancy with according to various factors (age, gender, and anatomical locations) within a human body [26–28]. Therefore, a scaffold is designed in such a way so that a balance between the porosity level and mechanical properties can be maintained [29–31]. This prevents the bone from stress shielding as well as reabsorption due to bone–scaffold interaction [32, 33]. TPMS-based porous scaffolds also enhance the bone ingrowth and weight-bearing capacity due to their exceptional porous architecture that are lightweight in comparison with the conventional solid scaffolds [12, 33–35].

Figure 80.5 characterizes the mechanical properties comprising the effective elastic moduli along with stress distribution for primitive and gyroid surface models with varying porosity under a compressive load of 75 N in inverse Y direction. Effective elastic modulus and compressive strength for both structures (primitive and gyroid) was maximum for minimum porosity of 60% and followed a pattern to decrease with increasing porosity.

Observing the characteristics of effective elastic moduli (Fig. 80.5a), a maximum effective elastic modulus of 43.73 MPa for P surface and 39.36 MPa for gyroid surface was obtained in case of 60% porosity. However, a minimum value of 6.625 MPa for P surface and 5.628496 MPa for gyroid surface was obtained in case of maximum porosity of 90%.

Likewise, the compressive strength (Fig. 80.5b) was also observed to be maximum in case of 60% porosity for both primitive surface (100.519 MPa) and gyroid surface (96.029 MPa). A minimum value of von-Mises stress was obtained in case of 90% porosity for primitive surface (25.52178 MPa) and gyroid surface (21.06333 MPa). However, it can be noted that, for 80% porosity, the compressive strength was approximately equal for P surface (49.78 MPa) and gyroid surface (48.68 MPa).

As a result, it can be concluded that effective elastic moduli of gyroid surface models were lower than P surface models for all the porosity levels. Similar to the pattern of effective elastic moduli, compressive strength was also observed to be low for gyroid surface models as compared to P surface models for all the porosity levels ranging from 60 to 90%.

Fig. 80.6 Illustration of mapping of developed porous scaffold to treat large segmental bone defect
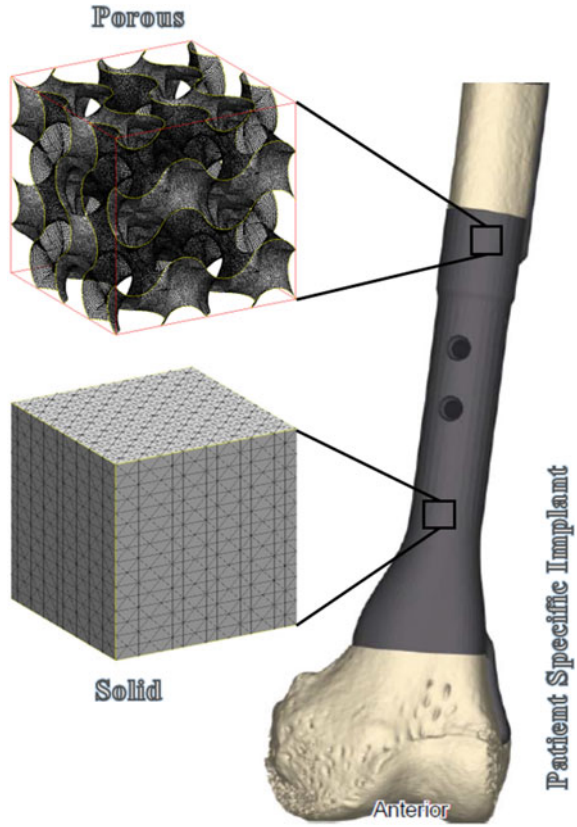
The conclusions of this pre-clinical analysis study elucidated the proficiency of design criterion for selecting an efficient scaffold structure in order to obtain the preferred value of the mechanical properties intended for patient-specific implant manufacturing that can be used for treating large segmental bone defects [36], where high porosity scaffolds are greatly needed (Fig. 80.6).

The overview of outcomes achieved in accordance with the mechanical properties of TPMS-based porous scaffold recommended their applicability at different anatomical locations according to the porosity level and suggested them to be appropriate structures for applications in bridging the bone gaps. However, the result is effective merely for desired scaffold structure requirements. The working fundamentals can be followed for other porous scaffold structures and biomechanical bone properties.

References

1. Almeida, H.A.: Design of tissue engineering scaffolds based on hyperbolic surfaces: structural numerical evaluation. Med. Eng. Phys. **36**(8), 1033–1040 (2014)
2. Zhang, X.Y.: Additively manufactured scaffolds for bone tissue engineering and the prediction of their mechanical behavior: a review. Materials **10**(1), 50 (2017)
3. Yang, N.: Mathematically defined gradient porous materials. Mater. Lett. **173**, 136–140 (2016)
4. Melchels, F.P.: Mathematically defined tissue engineering scaffold architectures prepared by stereolithography. Biomaterials **31**(27), 6909–6916 (2010)
5. Bobbert, F.S.L.: Additively manufactured metallic porous biomaterials based on minimal surfaces: a unique combination of topological, mechanical, and mass transport properties. Acta Biomater. **53**, 572–584 (2017)
6. Mehboob, H.: Finite element modelling and characterization of 3D cellular microstructures for the design of a cementless biomimetic porous hip stem. Mater. Des. **149**, 101–112 (2018)
7. Mohammed, M.I.: Design of three-dimensional, triply periodic unit cell scaffold structures for additive manufacturing. J. Mech. Des. **140**(7), 071701 (2018)
8. Mohammed, M.I.: Design and fabrication considerations for three dimensional scaffold structures. KnE Eng. **2**(2), 120–126 (2017)
9. Zheng, X.: Minimal surface designs for porous materials: from microstructures to mechanical properties. J. Mater. Sci. **53**(14), 10194–10208 (2018)
10. Blanquer, S.B.: Surface curvature in triply-periodic minimal surface architectures as a distinct design parameter in preparing advanced tissue engineering scaffolds. Biofabrication **9**(2), 025001 (2017)
11. Feng, J.: Porous scaffold design by solid T-splines and triply periodic minimal surfaces. Comput. Methods Appl. Mech. Eng. **336**, 333–352 (2018)
12. Wang, S.: Lightweight of artificial bone models utilizing porous structures and 3D printing. Int. J. Performability Eng. **13**(5), 633 (2017)
13. Olivares, A.L.: Finite element study of scaffold architecture design and culture conditions for tissue engineering. Biomaterials **30**(30), 6142–6149 (2009)
14. Melchels, F.P.: A poly (D, L-lactide) resin for the preparation of tissue engineering scaffolds by stereolithography. Biomaterials **30**(23–24), 3801–3809 (2009)
15. Gauvin, R.: Microfabrication of complex porous tissue engineering scaffolds using 3D projection stereolithography. Biomaterials **33**(15), 3824–3834 (2012)
16. Giannitelli, S.M.: Current trends in the design of scaffolds for computer-aided tissue engineering. Acta Biomater. **10**(2), 580–594 (2014)
17. Maskery, I.: Insights into the mechanical properties of several triply periodic minimal surface lattice structures made by polymer additive manufacturing. Polymer **152**, 62–71 (2018)
18. Li, X.: Fabrication and characterization of porous Ti6Al4V parts for biomedical applications using electron beam melting process. Mater. Lett. **63**(3–4), 403–405 (2009)
19. Welsch, G., Boyer, R., Collings, E.W. (eds.): Materials properties handbook: titanium alloys. ASM international (1993)
20. Walker, J.M.: Design and mechanical characterization of solid and highly porous 3D printed poly (propylene fumarate) scaffolds. Prog. Addit. Manuf. **2**(1–2), 99–108 (2017)
21. Dias, M.R.: Optimization of scaffold design for bone tissue engineering: a computational and experimental study. Med. Eng. Phys. **36**(4), 448–457 (2014)
22. Murr, L.E.: Next-generation biomedical implants using additive manufacturing of complex, cellular and functional mesh arrays. Philos. Trans. R. Soc. Lond. A: Math. Phys. Eng. Sci. **368**(1917), 1999–2032 (2010)
23. Al-Ketan, O.: Mechanical properties of a new type of architected interpenetrating phase composite materials. Adv. Mater. Technol. **2**(2), 1600235 (2017)
24. Montazerian, H.: Porous scaffold internal architecture design based on minimal surfaces: a compromise between permeability and elastic properties. Mater. Des. **126**, 98–114 (2017)

25. Wang, X.: Topological design and additive manufacturing of porous metals for bone scaffolds and orthopaedic implants: a review. Biomaterials **83**, 127–141 (2016)
26. Choi, K.: The elastic moduli of human subchondral, trabecular, and cortical bone tissue and the size-dependency of cortical bone modulus. J. Biomech. **23**(11), 1103–1113 (1990)
27. Rho, J.Y.: Mechanical properties and the hierarchical structure of bone. Med. Eng. Phys. **20**(2), 92–102 (1998)
28. Rho, J.Y.: Young's modulus of trabecular and cortical bone material: ultrasonic and microtensile measurements. J. Biomech. **26**(2), 111–119 (1993)
29. Li, D.: Optimal design and modeling of gyroid-based functionally graded cellular structures for additive manufacturing. Comput. Aided Des. **104**, 87–99 (2018)
30. Ataee, A.: Anisotropic Ti-6Al-4V gyroid scaffolds manufactured by electron beam melting (EBM) for bone implant applications. Mater. Des. **137**, 345–354 (2018)
31. Kadkhodapour, J.: Failure mechanisms of additively manufactured porous biomaterials: effects of porosity and type of unit cell. J. Mech. Behav. Biomed. Mater. **50**, 180–191 (2015)
32. Arabnejad, S.: Fully porous 3D printed titanium femoral stem to reduce stress-shielding following total hip arthroplasty. J. Orthop. Res. **35**(8), 1774–1783 (2017)
33. Arabnejad, S.: High-strength porous biomaterials for bone replacement: a strategy to assess the interplay between cell morphology, mechanical properties, bone ingrowth and manufacturing constraints. Acta Biomater. **30**, 345–356 (2016)
34. Kadkhodapour, J.: Investigating internal architecture effect in plastic deformation and failure for TPMS-based scaffolds using simulation methods and experimental procedure. Mater. Sci. Eng., C **43**, 587–597 (2014)
35. Taniguchi, N.: Effect of pore size on bone ingrowth into porous titanium implants fabricated by additive manufacturing: an in vivo experiment. Mater. Sci. Eng., C **59**, 690–701 (2016)
36. Reichert, J.C.: The challenge of establishing preclinical models for segmental bone defect research. Biomaterials **30**(12):2149–2163 (2009)